basic research www.kidney-international.org

Bone marrow transplantation improves proximal tubule dysfunction in a mouse model of Dent disease

see commentary on page 776

Sarah S. Gabriel[1,2,4], Hendrica Belge[1,4], Alkaly Gassama[1,4], Huguette Debaix[1], Alessandro Luciani[1], Thomas Fehr[1,2,3] and Olivier Devuyst[1]

[1]*Institute of Physiology, University of Zürich, Zürich, Switzerland;* [2]*Division of Nephrology, University Hospital Zürich, Zürich, Switzerland; and* [3]*Department of Internal Medicine, Cantonal Hospital Graubünden, Chur, Switzerland*

Dent disease is a rare X-linked tubulopathy caused by mutations in the endosomal chloride-proton exchanger (ClC-5) resulting in defective receptor-mediated endocytosis and severe proximal tubule dysfunction. Bone marrow transplantation has recently been shown to preserve kidney function in cystinosis, a lysosomal storage disease causing proximal tubule dysfunction. Here we test the effects of bone marrow transplantation in *Clcn5*$^{Y/-}$ mice, a faithful model for Dent disease. Transplantation of wild-type bone marrow in *Clcn5*$^{Y/-}$ mice significantly improved proximal tubule dysfunction, with decreased low-molecular-weight proteinuria, glycosuria, calciuria, and polyuria four months after transplantation, compared to *Clcn5*$^{Y/-}$ mice transplanted with ClC-5 knockout bone marrow. Bone marrow–derived cells engrafted in the interstitium, surrounding proximal tubule cells, which showed a rescue of the apical expression of ClC-5 and megalin receptors. The improvement of proximal tubule dysfunction correlated with *Clcn5* gene expression in kidneys of mice transplanted with wild-type bone marrow cells. Coculture of *Clcn5*$^{Y/-}$ proximal tubule cells with bone marrow–derived cells confirmed rescue of ClC-5 and megalin, resulting in improved endocytosis. Nanotubular extensions between the engrafted bone marrow–derived cells and proximal tubule cells were observed *in vivo* and *in vitro*. No rescue was found when the formation of the tunneling nanotubes was prevented by actin depolymerization or when cells were physically separated by transwell inserts. Thus, bone marrow transplantation may rescue the epithelial phenotype due to an inherited endosomal defect. Direct contacts between bone marrow–derived cells and diseased tubular cells play a key role in the rescue mechanism.

Kidney International (2017) **91,** 842–855; http://dx.doi.org/10.1016/j.kint.2016.11.016

Correspondence: *Olivier Devuyst, Institute of Physiology, University of Zürich, Winterthurerstrasse 190, 8057 Zürich, Switzerland. E-mail: olivier.devuyst@uzh.ch*

[4]These authors contributed equally to the study.

Received 12 August 2016; revised 1 November 2016; accepted 23 November 2016; published online 28 January 2017

KEYWORDS: bone marrow cell; ClC-5; low-molecular weight proteinuria; proximal tubule; renal Fanconi syndrome

The epithelial cells lining the proximal tubules (PTs) of the kidney constitute a paradigm of effective communication between the external environment and the endomembrane system.[1] By processing incoming substances and recycling receptors and transporters at the apical membrane, the connecting endolysosomal system governs the terminal differentiation of PT cells and the recovery of essential substances that would otherwise be lost in the urine.[2] These substances include low-molecular-weight (LMW) proteins, which are filtered and then completely reabsorbed by apical endocytosis involving the multiligand receptors megalin and cubilin. After binding and internalization, ligands are delivered to endosomes and further to lysosomes for processing and degradation so that PT cells play a pivotal role in homeostasis.[3] Alterations in these transport processes can lead to generalized PT dysfunction (renal Fanconi syndrome), characterized by urinary loss of solutes including LMW proteins, glucose, and phosphate and is often complicated by dehydration, electrolyte imbalance, rickets, and development of chronic kidney disease. Such PT dysfunction is typically encountered in congenital disorders of the endolysosomal compartment, including Dent disease and nephropathic cystinosis.[4]

Dent disease (MIM #300009) is a rare, X-linked disorder characterized by LMW proteinuria, generalized PT dysfunction, kidney stones, and renal failure.[5] The disease is caused by inactivating mutations of the *CLCN5* gene that encodes ClC-5, an electrogenic Cl^-/H^+ exchanger that is located in the early endosomes of PT cells,[6] where it regulates vesicular Cl^- concentration, potentially affecting the activity of the vacuolar H^+-ATPase and/or vesicle recycling.[7] Studies in *Clcn5*$^{Y/-}$ mice, which represent a well-established model of Dent disease, demonstrated that the functional loss of ClC-5 induced a severe loss of megalin and cubilin at the brush border membrane, with impaired endocytosis and lysosomal processing of internalized ligands in PT cells.[8,9] The defective endocytosis and apical transport processes explain why

solutes are lost in the urine, often resulting in renal Fanconi syndrome. In the absence of therapy targeting the molecular defect, the current care of patients with Dent disease is solely supportive, focusing on the prevention of metabolic complications and nephrolithiasis.

Recently, bone marrow (BM) and hematopoietic stem cell (HSC) transplantation have been shown to preserve kidney function in nephropathic cystinosis, the most frequent cause of renal Fanconi syndrome in children.[10,11] Cystinosis (MIM #219800) is caused by autosomal recessive mutations in the *CTNS* gene, which encodes cystinosin, a lysosomal cystine-H^+ cotransporter exporting cystine into the cytosol. Functional loss of cystinosin results in lysosomal accumulation of cystine crystals leading to progressive dysfunction of multiple organs including the kidney. In children with nephropathic cystinosis, the most severe and frequent form of cystinosis, PT dysfunction and renal Fanconi syndrome develop before 1 year of age, often followed by chronic kidney disease.[12] Healthy BM-derived cells decreased cystine levels in the kidneys of diseased mice and improved several serum and urinary parameters in relation to the level of engraftment.[11] Subsequently, *in vitro* studies suggested that vesicular cross-correction mediated by transfer of cystinosin-bearing lysosomes could sustain the correction.[13,14] Whether BM transplantation could improve the epithelial phenotype in other congenital defects of the endolysosomal pathway, in particular those that are not associated with lysosomal storage, is unknown. Furthermore, the mechanism of rescue, without evidence of target tissue differentiation and replacement of damaged cells, remains a major issue in stem cell transplantation.[15]

Based on the encouraging results in cystinosis, we tested the effects of BM transplantation in the well-established $Clcn5^{Y/-}$ mouse model of Dent disease and used a coculture system to analyze the potential mechanisms involved.

RESULTS

Protocol and hematopoietic chimerism

To test whether BM transplantation improves the PT dysfunction associated with Dent disease, we transplanted 10-week-old ClC-5 knockout (KO) male ($Clcn5^{Y/-}$) mice with wild-type (WT) (GFP)–expressing BM cells ("treated"). As controls, $Clcn5^{Y/-}$ mice were transplanted with KO-BM cells from $Clcn5^{Y/-}$ mice ("negative controls") and age- and sex-matched WT littermates ($Clcn5^{Y/+}$) were transplanted with WT-BM cells ("positive controls") (Figure 1a). Urine and plasma were collected at baseline (1 week before transplantation) and then 10 weeks and 16 weeks after transplantation. Because recipients were lethally irradiated per protocol, BM transplantation resulted in full multilineage hematopoietic chimerism in peripheral blood in all mice, as shown by a nearly 100% myeloid and B-cell chimerism (Figure 1b).

Improvement of PT dysfunction in $Clcn5^{Y/-}$ mice transplanted with BM cells

As previously described,[9,16] $Clcn5^{Y/-}$ mice exhibited features of PT dysfunction including polyuria, glycosuria, hypercalciuria, and LMW proteinuria (detection of 16-kD Clara cell protein [CC16]) compared with WT littermates at baseline (Table 1).

In order to assess the potential effect of BM transplantation, we analyzed markers of PT dysfunction over time

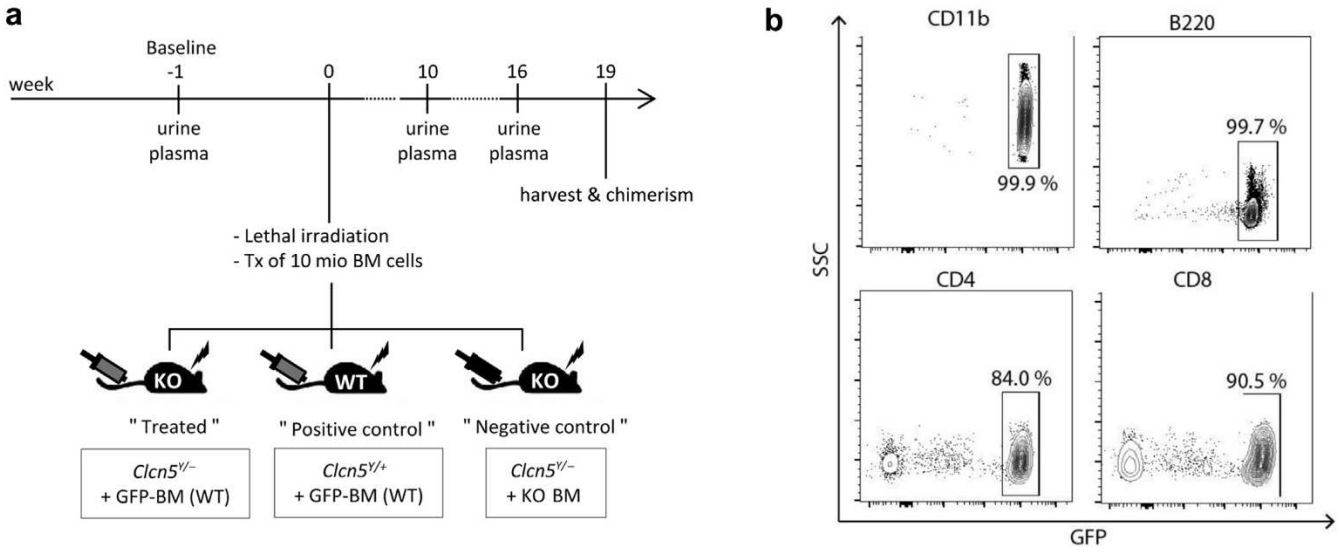

Figure 1 | Study design and peripheral blood chimerism. (**a**) Experimental setup of the study. $Clcn5^{Y/-}$ and $Clcn5^{Y/+}$ littermates were transplanted at the age of 10 weeks with either wild-type (WT, $Clcn5^{Y/+}$) GFP+ or knockout (KO, $Clcn5^{Y/-}$) bone marrow (BM) cells. Baseline blood sampling and urine collection (overnight) were performed the week before BM transplantation and 10 and 16 weeks after BM transplantation. (**b**) Lineage-specific peripheral blood chimerism was measured by FACS analysis of GFP+ cells at the time of kidney harvest. A nearly 100% myeloid and B-cell chimerism was observed. FACS, fluorescence-activated cell sorting; GFP, green fluorescent protein; mio, millions of BM cells; SSC, side-scatter light, a parameter proportional to cell granularity used for FACS analysis; Tx, transplantation.

in treated versus negative control *Clcn5*$^{Y/-}$ mice (Figure 2, Table 1). Over the 16-week observation period, the negative controls (*Clcn5*$^{Y/-}$ mice transplanted with KO-BM) showed a significant increase in diuresis and urinary excretion of CC16, pointing toward progression of the disease over time. In contrast, the transplanted *Clcn5*$^{Y/-}$ mice showed no significant change in diuresis and a significant *reduction* (~30% decrease) in the urinary excretion of CC16. Similarly, glycosuria and calciuria decreased significantly in transplanted animals, whereas these parameters were unchanged in negative controls. These data show a significant improvement of PT dysfunction in mice transplanted with WT BM cells compared with negative controls.

The biological effect of BM transplantation was reflected by the engraftment of BM-derived cells into *Clcn5*$^{Y/-}$ kidneys (Figure 3). The *Clcn5*$^{Y/-}$ mice displayed a significantly higher recruitment of GFP+ BM–derived cells into the kidneys than *Clcn5*$^{Y/+}$ mice, at the mRNA and protein levels and confirmed by immunofluorescence for GFP (Figure 3a,b).

Recovery of megalin and ClC-5 in kidneys of BM-transplanted *Clcn5*$^{Y/-}$ mice

Because filtered LMW proteins are reabsorbed by receptor-mediated endocytosis in PT cells, the reduced urinary loss of CC16 in transplanted mice suggests that the endocytic machinery is at least partially recovered. To test this hypothesis, we investigated the expression level of megalin in the kidneys (Figure 4). Contrasting with the selective loss of megalin expression observed in control *Clcn5*$^{Y/-}$ versus *Clcn5*$^{Y/+}$ kidneys, a strong rescue of megalin expression was detected by Western blot in *Clcn5*$^{Y/-}$ kidneys of mice transplanted with WT BM cells (Figure 4a). The rescue of megalin was specific because the expression of aquaporin-1 and the endosome catalyst Rab5 remained unchanged in all treatment groups. Of note, BM transplantation had no effect on protein expression in any genotype.

The rescue of megalin was confirmed by immunofluorescence staining of the kidneys in BM-transplanted mice (Figure 4b). Whereas almost no megalin staining could be detected in *Clcn5*$^{Y/-}$ kidneys transplanted with KO-BM cells, an appreciable rescue of megalin was observed in the brush border of PT cells in *Clcn5*$^{Y/-}$ kidneys transplanted with WT BM cells.

In parallel, a significant rescue of ClC-5 expression was observed in *Clcn5*$^{Y/-}$ kidneys of mice transplanted with WT BM cells, as shown by immunoblot (Figure 4a) and real-time polymerase chain reaction (qPCR) (Figure 4c). The rescued ClC-5 in treated *Clcn5*$^{Y/-}$ kidneys was confirmed by immunofluorescence staining at the brush border of PT cells (Figure 4b) and at high magnification in subapical vesicles reminiscent of endosomes (Supplementary Figure S1A). The staining for ClC-5 was partially overlapping with that of megalin in PT cells (Supplementary Figure S2). Of note, the degree of LMW proteinuria (monitored by the urinary loss of

Table 1 | Urine and plasma parameters at baseline and in transplanted *Clcn5*$^{Y/-}$ and *Clcn5*$^{Y/+}$ mice

	Clcn5$^{Y/-}$		*Clcn5*$^{Y/+}$	*P* value
Baseline	**(Negative controls) (n = 8–10)**	**(Treated) (n = 13–15)**	**(Positive controls) (n = 6–9)**	***Clcn5*$^{Y/-}$ versus *Clcn5*$^{Y/+}$**
Diuresis (ml/12 h)	1.98 ± 0.26[a]	2.04 ± 0.21[a]	1.20 ± 0.19	<0.01
U CC16 (mg/g creat)	62.3 ± 4.3	66.7 ± 5.3	ND	ND
U glucose (mg/12 h)	1.21 ± 0.15[a]	1.44 ± 0.14[a]	0.49 ± 0.06	<0.0001
U Ca^{2+} (mg/g creat)	216 ± 29[a]	196 ± 12[a]	83 ± 5	<0.0001
BUN (mg/dl)	24.5 ± 1.2	24.3 ± 1.1	25.1 ± 1.7	NS
Week 10	***Clcn5*$^{Y/-}$ + KO-BM (negative controls)**	***Clcn5*$^{Y/-}$ + GFP-BM (treated)**	***Clcn5*$^{Y/+}$ + GFP-BM (positive controls)**	***P* value**
Diuresis (ml/12 h)	4.07 ± 0.64[a]	4.04 ± 0.84[a]	1.31 ± 0.19	0.0001
U CC16 (mg/g creat)	66.6 ± 5.5	53.9 ± 6.0	ND	0.087
U glucose (mg/12 h)	1.07 ± 0.18[a]	1.07 ± 0.16[a]	0.40 ± 0.08	0.0006
U Ca^{2+} (mg/g creat)	160 ± 26	132 ± 13	111 ± 36	0.13
BUN (mg/dl)	26.8 ± 1.7	25.0 ± 1.3	24.1 ± 1.2	0.54
Week 16	***Clcn5*$^{Y/-}$ + KO-BM (negative controls)**	***Clcn5*$^{Y/-}$ + GFP-BM (treated)**	***Clcn5*$^{Y/+}$ + GFP-BM (positive controls)**	***P* value**
Diuresis (ml/12 h)	6.04 ± 1.52[a]	3.36 ± 0.92[a]	1.03 ± 0.24	0.0002
U CC16 (mg/g creat)	71.2 ± 3.5	46.9 ± 5.1[b]	ND	0.0031
U glucose (mg/12 h)	0.87 ± 0.10[a]	0.81 ± 0.12[a]	0.36 ± 0.07	0.0023
U Ca^{2+} (mg/g creat)	146 ± 21[a]	131 ± 10[a]	99 ± 31	0.0126
BUN (mg/dl)	24.6 ± 1.4	24.7 ± 0.9	23.4 ± 1.5	0.70

BM, bone marrow; BUN, blood urea nitrogen; CC16, Clara cell protein of 16 kDa; creat, creatinine; GFP, green fluorescent protein; KO, knockout; ND, not detected; NS, not significant; P, plasma; U, urine.
Baseline parameters: Mann-Whitney test (*Clcn5*$^{Y/-}$ vs *Clcn5*$^{Y/+}$); weeks 10 and 16: 1-way analysis of variance nonparametric (Kruskal-Wallis test) for all parameters except U CC16 (Mann-Whitney test).
[a]$P < 0.05$ versus *Clcn5*$^{Y/+}$ (baseline) + green fluorescent protein-labeled bone marrow (weeks 10 and 16).
[b]$P < 0.05$ versus *Clcn5*$^{Y/-}$ + knockout bone marrow.

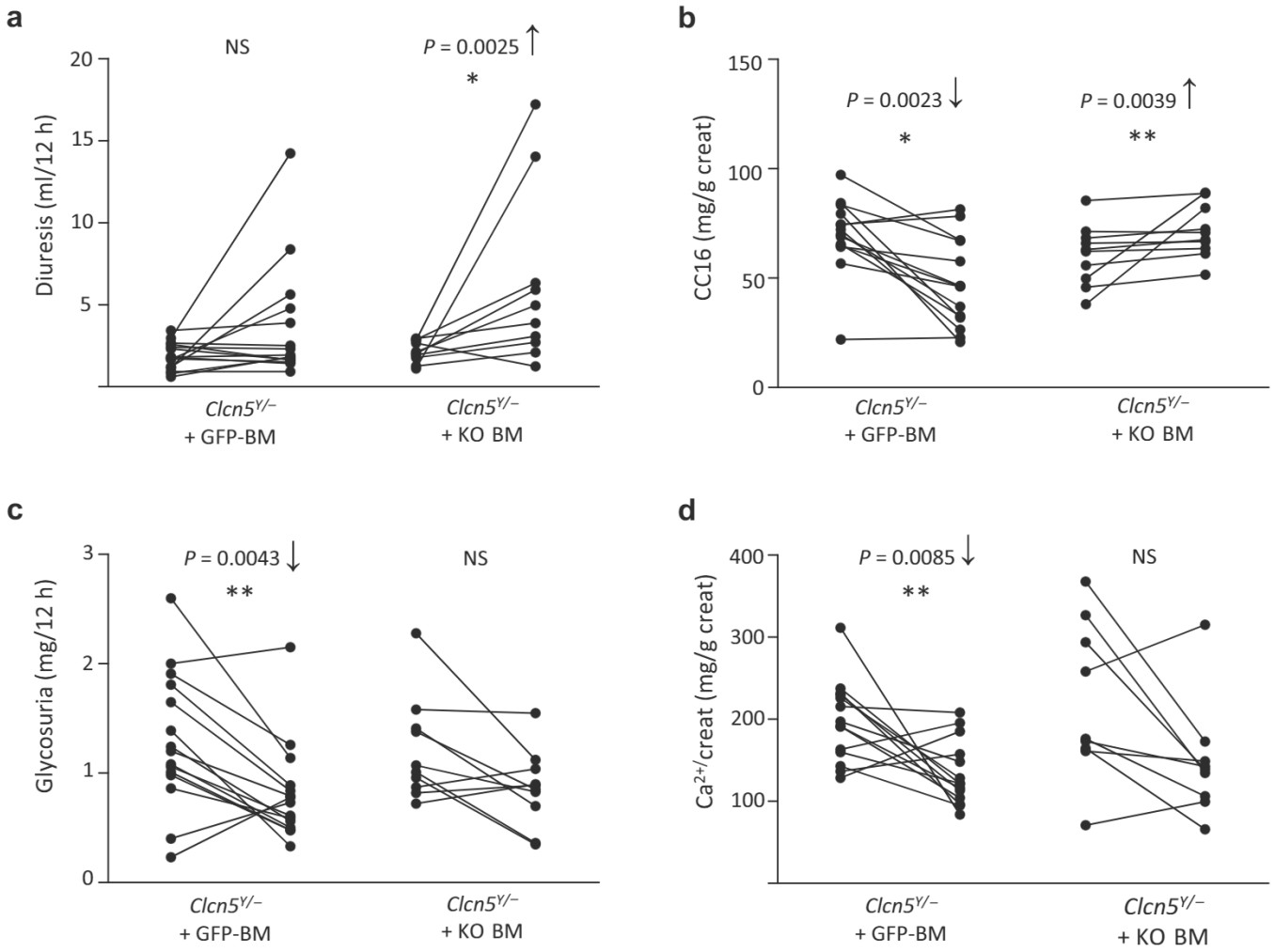

Figure 2| Evolution of urinary parameters after bone marrow (BM) transplantation in *Clcn5*$^{Y/-}$ mice. Evolution (baseline to week 16) of urinary parameters (diuresis, urinary excretion of the low-molecular-weight protein CC16, glycosuria, and calciuria) in *Clcn5*$^{Y/-}$ mice transplanted with either wild-type (WT) (*Clcn5*$^{Y/+}$) GFP+ or KO (*Clcn5*$^{Y/-}$) BM cells. The *Clcn5*$^{Y/-}$ mice transplanted with WT BM cells showed no significant change in diuresis (**a**) and a significant reduction in the urinary excretion of CC16 (**b**), in glycosuria (**c**) and calciuria (**d**) compared with increased or stable values in *Clcn5*$^{Y/-}$ mice transplanted with KO-BM cells. Differences in urinary parameters from baseline to week 16 were assessed with Wilcoxon signed rank test. *$P < 0.05$; **$P < 0.01$; CC16, Clara cell protein of 16 kDa; creat, creatinine; GFP-BM, green fluorescent protein bone marrow; KO-BM, knockout bone marrow; NS, not significant.

CC16) in the treated *Clcn5*$^{Y/-}$ mice inversely correlated with the level of ClC-5 mRNA rescued in the kidneys (Figure 4c).

Engrafted cells are mononuclear phagocytes that are closely associated with PT cells

To further investigate the mechanisms driving the improvement in PT dysfunction, we analyzed the location and identity of the BM-derived cells in *Clcn5*$^{Y/-}$ kidneys. Besides the fact that more BM-derived cells engrafted to the *Clcn5*$^{Y/-}$ versus *Clcn5*$^{Y/+}$ kidneys (Figure 3), the engrafted cells also showed a distinct distribution pattern. In *Clcn5*$^{Y/-}$ kidneys, the transplanted cells were found to be clustering around PT profiles, in close contact with PT cells, whereas in *Clcn5*$^{Y/+}$ kidneys, the transplanted cells were interspersed in the interstitium without clear contact with PT sections (Figure 5a). The different locations were confirmed by automated confocal image analysis, showing a lower average distance of GFP+ cells from PT cells in *Clcn5*$^{Y/-}$ versus *Clcn5*$^{Y/+}$ kidneys, respectively (Figure 5a).

The nature of the engrafted cells was then assessed (Figure 5b). All transplanted GFP+ cells were found in the interstitium. Because we transplanted a whole BM cell suspension (i.e., a mixture of HSCs, mesenchymal stromal cells, differentiated lymphocytes, and myeloid cells as well as their immature precursors), the engrafted cells may theoretically derive from mesenchymal stromal cells present in the suspension. Such cells do not migrate into healthy tissues, but on irradiation injury, increased recruitment into peripheral organs has been observed.[17] In case of acute injury, mesenchymal stromal cells have been recruited in the kidneys where they may persist for a long time.[18] However, with their characteristic protrusions, the GFP-expressing cells

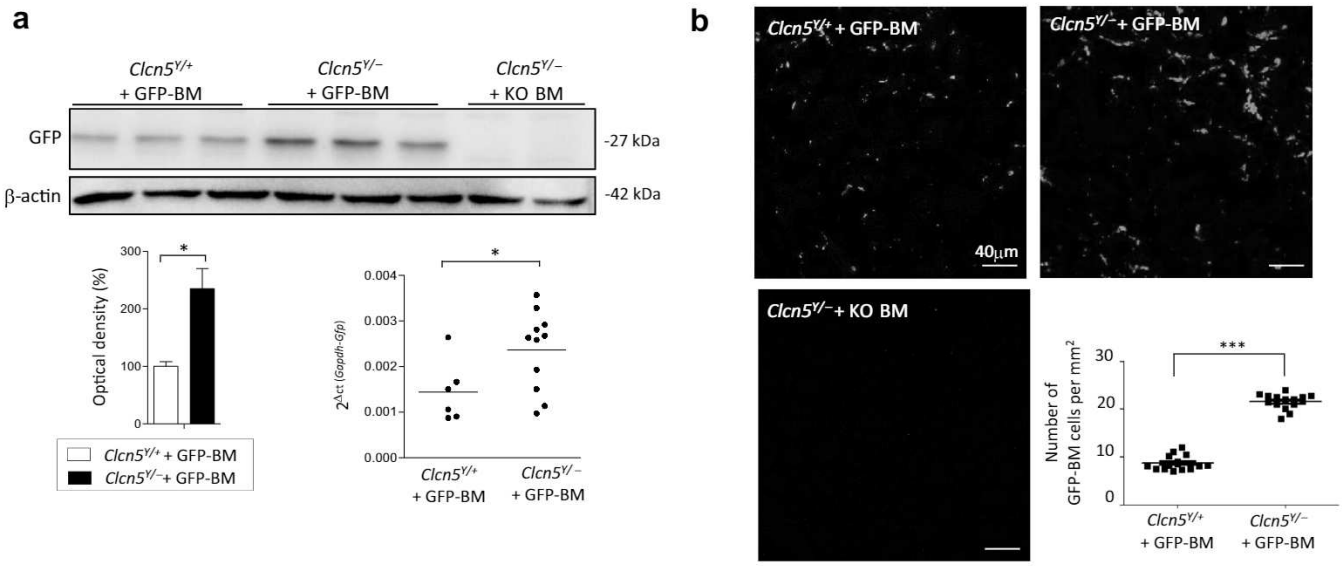

Figure 3 | Engraftment of transplanted bone marrow (BM) cells in *Clcn5* kidneys. (**a**) Western blot for green fluorescent protein (GFP) expression in kidney lysates of transplanted *ClCn5*$^{Y/+}$ and *ClCn5*$^{Y/-}$ mice. The lower panels show the densitometry of immunoblot signals and the real-time polymerase chain reaction (qPCR) analysis of *Gfp* mRNA expression in the *Clcn5*$^{Y/+}$ and *Clcn5*$^{Y/-}$ transplanted kidneys. The engraftment of BM-derived cells is significantly greater in the *Clcn5*$^{Y/-}$ transplanted kidneys. Statistical differences were assessed using the Mann-Whitney test. *$P < 0.05$. (**b**) Confocal microscopy images showing GFP expression in the kidneys of *Clcn5*$^{Y/+}$ and *Clcn5*$^{Y/-}$ mice that were transplanted with wild-type, GFP+ BM cells, or knockout-BM cells. The graph gives the quantification of GFP-BM cells/mm^2. ***$P < 0.001$.

phenotypically resembled dendritic cells (DCs) or macrophages rather than MSC-derived cells, which would be spindle-shaped and compact. As DCs and macrophages further possess overlapping functions during steady state in the kidney, these cells are often referred to as mononuclear phagocytes.[19] We confirmed this identity by staining the kidney sections for CD45, CD11c (a DC marker), and F4/80 (a macrophage marker) (Figure 5b). Costaining of these markers with GFP allowed us to conclude that these cells originated from the hematopoietic lineage. Conversely, there was no overlap between the GFP cells and the fibroblast marker α-smooth muscle actin (Figure 5b). Furthermore, the engraftment efficiency of WT GFP+ BM cells and KO-BM cells in *Clcn5*$^{Y/-}$ kidneys was similar, as shown in Supplementary Figure S3.

Rescue of receptor-mediated endocytosis in a coculture system

In order to substantiate the rescue of PT function as observed *in vivo*, we established a coculture system based on primary cultures of mouse PT cells (mPTCs) obtained from microdissected PT segments of *Clcn5*$^{Y/-}$ kidneys.[20] These cells were then cocultivated for 2 days with BM-derived DCs/macrophages (BM-DC/MΦ). These BM-DC/MΦ were generated by stimulating either WT (GFP+) or KO-BM cells for 7 days with granulocyte-macrophage colony-stimulating factor (30 ng/ml), resulting in a mixed population of adherent phagocytic cells (Figure 6a). Fully differentiated BM-DC/MΦ expressed CD45 and F4/80 (Figure 6b) as well as ClC-5 and megalin (Supplementary Figure S1B). During the differentiation process of freshly isolated BM cells into BM-DC/MΦ, gradual upregulation of mRNA encoding for ClC-5 (*Clcn5*), for the macrophage/DC markers F4/80 (*Adgre1*), CD45 (*Ptprc*), and CD11c (*Itgax*), and for the tunneling nanotube markers myosin Va (*Myo5a*) and M-Sec or TNFaip2 (*Tnfaip2*) was observed (Figure 6c).

Immunofluorescence staining revealed that, compared with *Clcn5*$^{Y/-}$ mPTCs cocultivated with KO-BM-DC/MΦ, coculture of *Clcn5*$^{Y/-}$ mPTCs with WT BM-DC/MΦ showed rescue of megalin and ClC-5 expression, particularly evident in mPTCs close to GFP+ cells (Figure 7a, upper panel). The recovery of megalin and ClC-5 expression was confirmed by Western blot (Figure 7a, lower panel), with a functional counterpart based on albumin (Alexa 647 Fluor bovine serum albumin [BSA]) uptake by the *Clcn5*$^{Y/-}$ mPTCs (Figure 7b). Compared with the very low level observed in *Clcn5*$^{Y/-}$ mPTCs cocultivated with KO-BM-DC/MΦ, there was a significant, ~50%, rescue of albumin uptake in *Clcn5*$^{Y/-}$ mPTCs cocultivated with WT BM-DC/MΦ, although this was still lower than the uptake by *Clcn5*$^{Y/+}$ mPTCs cocultivated with WT BM-DC/MΦ (Figure 7b).

Nanotubes mediate the interaction between transplanted BM-derived cells and PT cells

We finally investigated potential rescue mechanisms of PT dysfunction by the transplanted BM cells. Visualization of GFP provided evidence, both *in vivo* (Figure 8a–d) and *in vitro* (Figure 8e–g), for the existence of cellular prolongations between the GFP+ BM-derived cells and PT cells from the *Clcn5*$^{Y/-}$ kidneys. These cellular prolongations resemble the tunneling nanotubes that form intracellular bridges supporting the microtubule-mediated transfer of

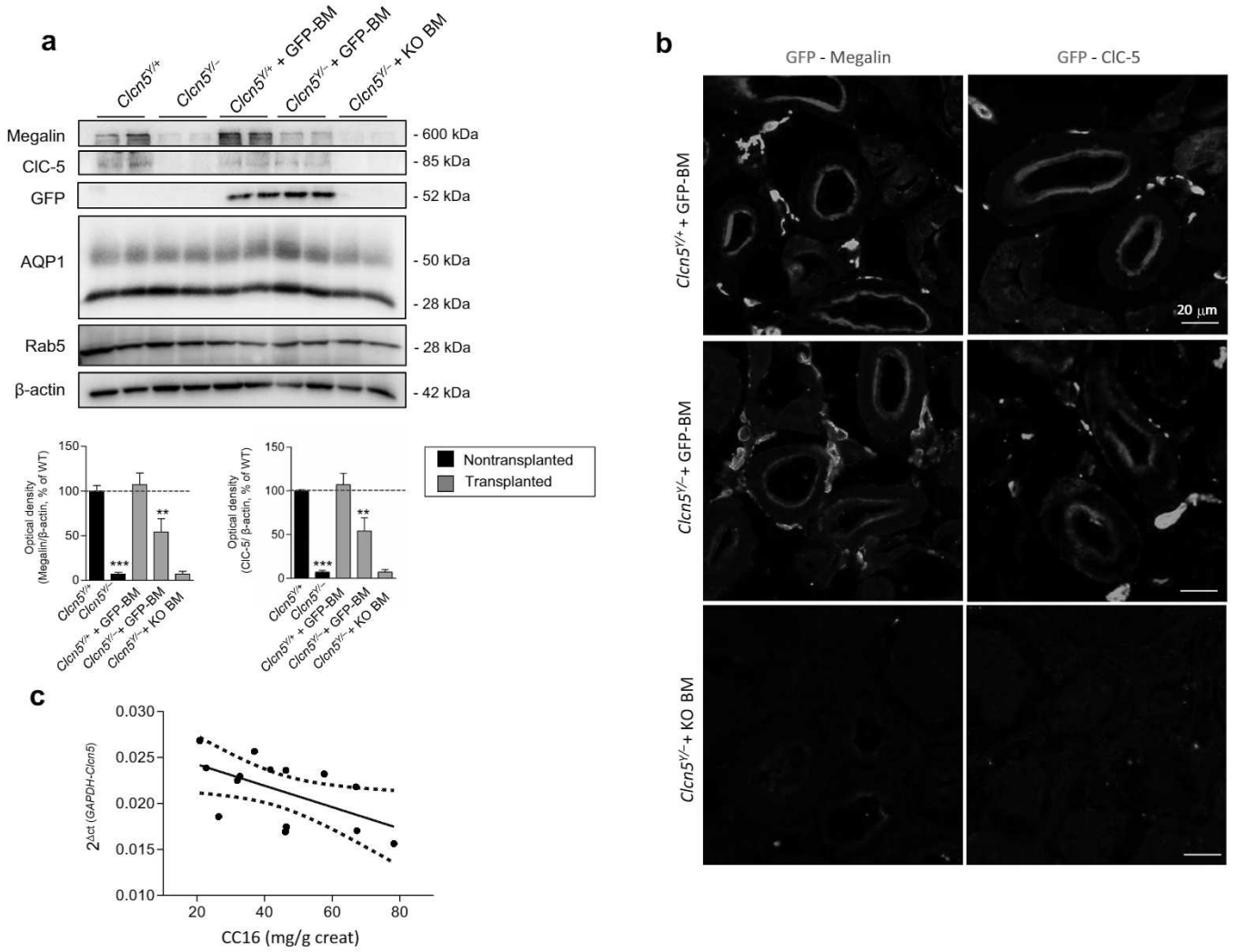

Figure 4 | Recovery of megalin and ClC-5 expression in *Clcn5*$^{Y/-}$ kidneys of bone marrow (BM)–transplanted mice. (**a**) Western blot for megalin, ClC-5, green fluorescent protein (GFP), aquaporin-1 (AQP1), and Rab5 in kidney lysates and quantification of optical density for megalin and ClC-5 in the lower panel. BM transplantation did not induce nonspecific effects on protein expression in *Clcn5*$^{Y/+}$ and *Clcn5*$^{Y/-}$ kidneys. A significant rescue of megalin and ClC-5 was detected in *Clcn5*$^{Y/-}$ kidneys of mice transplanted with wild-type (WT) GFP+ BM cells. Four animals per condition. ***$P < 0.001$ versus *Clcn5*$^{Y/+}$, **$P < 0.01$ versus *Clcn5*$^{Y/-}$ transplanted with knockout (KO) BM cells, Mann-Whitney test. (**b**) Confocal microscopy images showing staining for GFP (green), megalin (red, left panels), and ClC-5 (red, right panels) in *Clcn5*$^{Y/+}$ and *Clcn5*$^{Y/-}$ mice transplanted with WT GFP+ BM cells. Contrasting with the lack of ClC-5 and megalin staining in *Clcn5*$^{Y/-}$ kidneys of mice transplanted with KO-BM cells, an appreciable rescue of megalin in the brush border and ClC-5 in the apical region was observed in *Clcn5*$^{Y/-}$ kidneys of mice transplanted with WT BM cells. (**c**) Inverse correlation between the expression of *Clcn5* mRNA in *Clcn5*$^{Y/-}$ kidneys of mice transplanted with WT BM and the levels of urinary 16-kD Clara cell protein (CC16). A Mann-Whitney test was used to assess difference between treatment groups, and correlation represents a linear regression-model with 95% CI. There was no *Clcn5* mRNA signal in *ClCn5*$^{Y/-}$ kidneys of mice transplanted with KO-BM. GAPDH, glyceraldehyde-3-phosphate dehydrogenase.

intracellular components, as previously described in BM transplantation experiments.[14,21] Immunostaining experiments revealed that the GFP+ BM-derived cells established multiple contacts with PT cells in the *Clcn5*$^{Y/-}$ kidneys (Figure 8b) and that the nanotubes crossed the collagen type IV–positive tubular basement membrane to establish direct contact with PT cells (Figure 8c,d). In coculture experiments, multiple tunneling nanotubes positive for tubulin were identified between GFP+ BM BM-DC/MΦ cells and mPTCs derived from *Clcn5*$^{Y/-}$ mice (Figure 8e–g). A few GFP+ structures were also detected in PT cells in transplanted kidneys and in mPTCs in coculture (Supplementary Figure S4).

To explore the role of these nanotubular formations in the rescue mechanism, we blocked their formation by treating the mPTCs with the actin-depolymerizing agent latrunculin B.[21] This treatment prevented the development of cellular prolongations (Figure 8h), as well as the rescue of megalin and ClC-5 expression (Figure 8i) and the recovery of endocytosis activity (Alexa 647-BSA uptake) in cocultures of GFP+ BM-derived cells with *Clcn5*$^{Y/-}$ mPTCs (Figure 8h). Furthermore, when the *Clcn5*$^{Y/-}$ mPTCs were separated from the GFP+

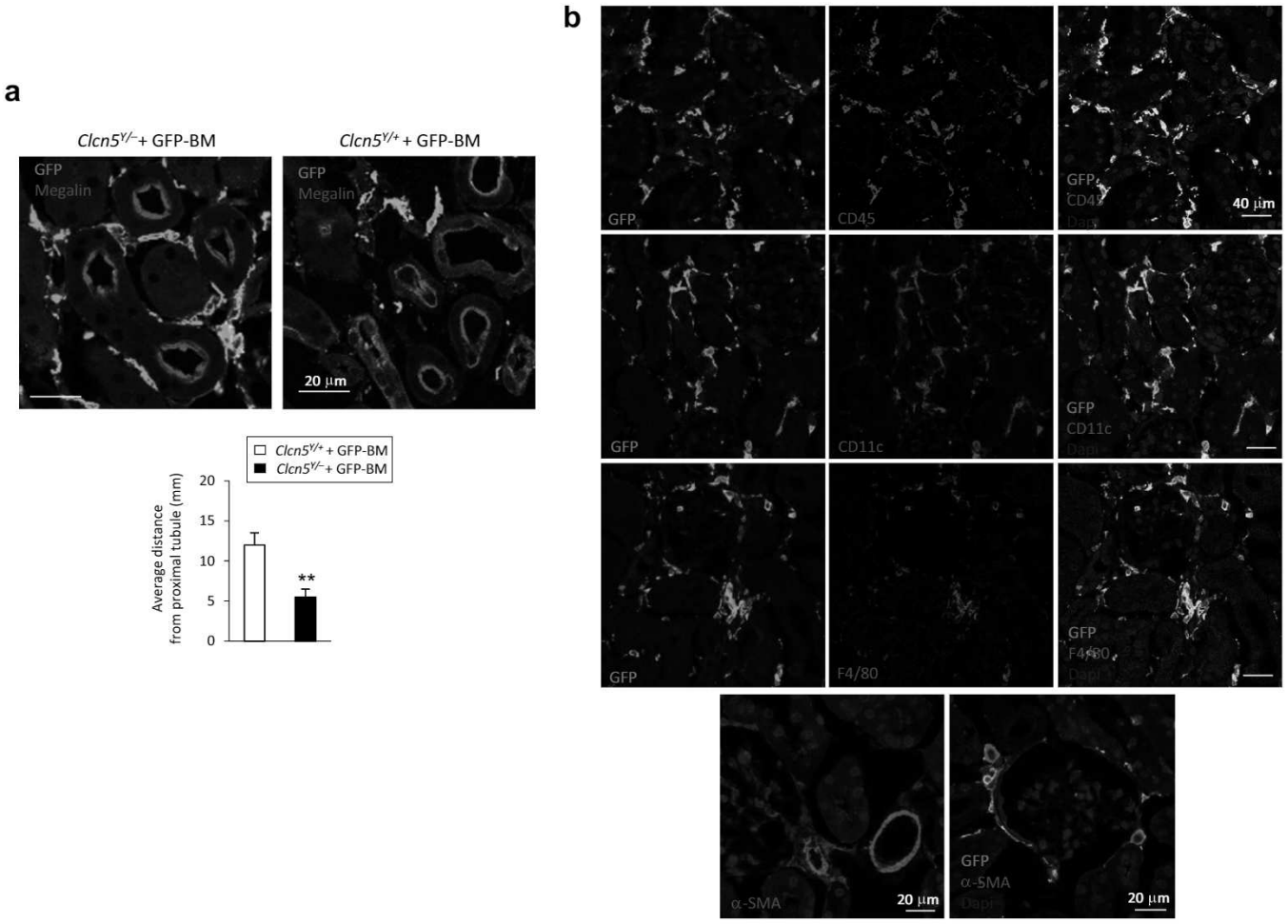

Figure 5 | Characterization and distribution of bone marrow (BM)–derived cells in *Clcn5* kidneys. (**a**) Confocal microscopy images showing staining for megalin (red) and green fluorescent protein (GFP) (green) in kidney sections of $Clcn5^{Y/-}$ (left panel) and $Clcn5^{Y/+}$ (right panel) mice transplanted with GFP+ BM cells. Bottom panel: The average distance of GFP+ BM cells in relation to (megalin-positive) proximal tubule (PT) cells in transplanted kidneys. In $Clcn5^{Y/-}$ kidneys, a higher number of transplanted GFP+ cells surround the PT profiles and are closer to PT cells compared with $Clcn5^{Y/+}$ kidneys in which fewer GFP+ cells are engrafted. $^{**}P < 0.01$, Mann-Whitney test. (**b**) Staining for GFP (green); 4′,6-diamidino-2-phenylindole (DAPI) (blue); mononuclear phagocyte markers CD45, CD11c, and F4/80 (red); and the fibroblast marker α-smooth muscle actin (α-SMA, red) in kidneys of $Clcn5^{Y/-}$ mice transplanted with GFP+ BM cells. The GFP+ BM–derived cells costain with CD45, CD11c, and F4/80, identifying these cells as mononuclear phagocytes. There is no overlap between the GFP cells and the fibroblast marker α-SMA.

BM-derived cells by using a transwell porous insert, we could not observe any rescue of the endocytic activity (Figure 8j). Taken together, these data suggest that the establishment of a direct contact between transplanted BM-derived cells and diseased PT cells, via tunneling nanotubes, plays a key role in the rescue.

DISCUSSION

The results presented here demonstrate for the first time that BM transplantation may rescue the epithelial phenotype caused by a genetic defect in an endosomal transporter. Transplantation of WT $Clcn5^{Y/+}$ BM cells to $Clcn5^{Y/-}$ mice significantly reduced the progression of LMW proteinuria, glycosuria, calciuria, and polyuria compared with $Clcn5^{Y/-}$ mice transplanted with KO $Clcn5^{Y/-}$ BM. The BM-derived cells differentiated into mononuclear phagocytes engrafted into the interstitium, surrounding PT cells to which they connected via nanotubular prolongations. The rescue of the epithelial phenotype is reflected by the recovery of ClC-5 and megalin expression in PT cells of $Clcn5^{Y/-}$ mice. Coculture of $Clcn5^{Y/-}$-derived PT cells with WT BM-derived cells confirmed the recovery of ClC-5 and megalin and that of receptor-mediated endocytosis. The rescue was abolished when the formation of tunneling nanotubes was prevented *in vitro*.

Although the value of BM and HSC transplantation is clearly established for malignant and genetic diseases of the hematopoietic system (e.g., acute leukemia, sickle cell disease, or severe combined immunodeficiency), it has also been successfully used for some types of lysosomal storage diseases. Lysosomal storage diseases are a group of diseases that are characterized by enzyme deficiency in lysosomes, resulting in substrate accumulation and subsequent cellular dysfunction. Here, healthy cells derived from the transplanted

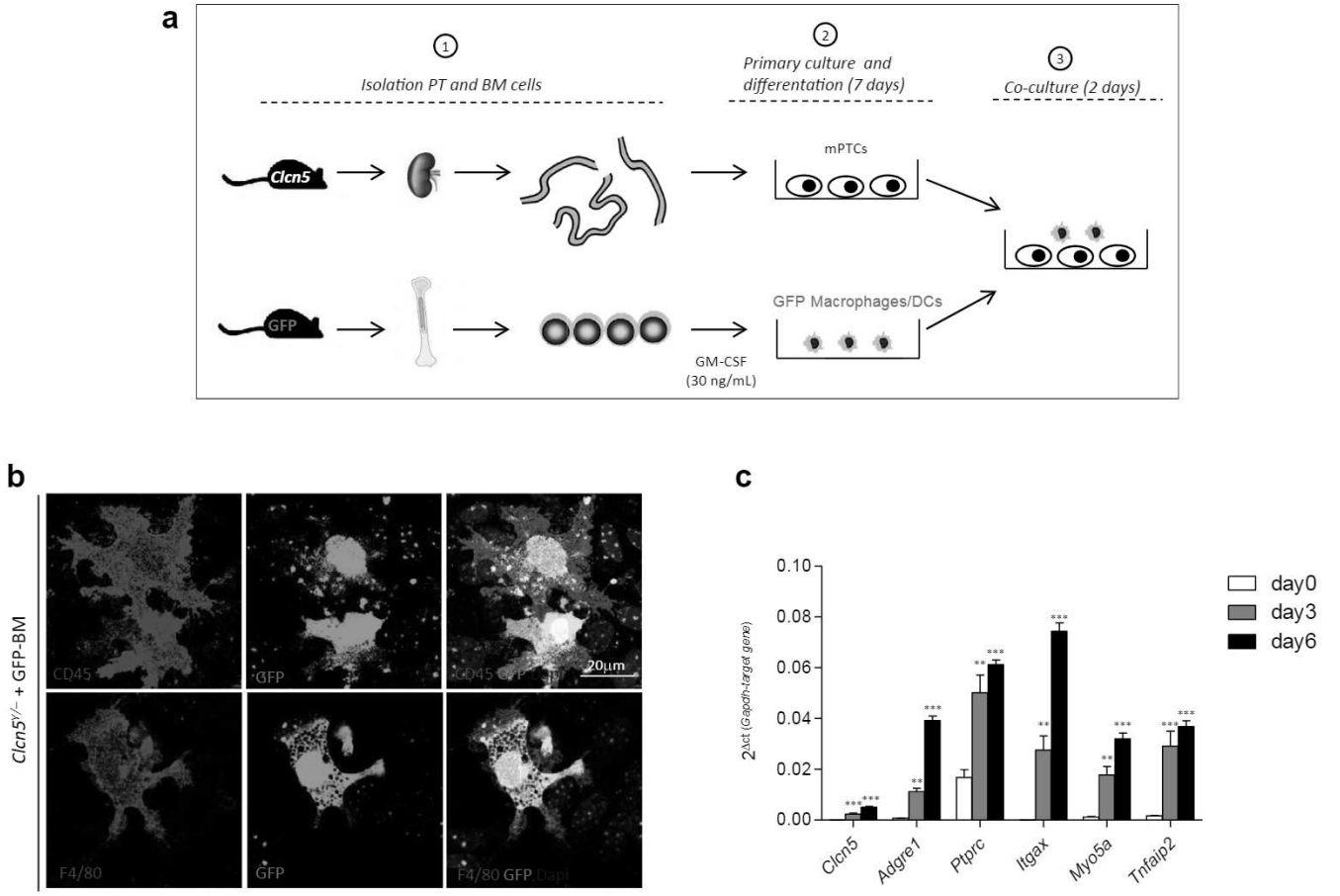

Figure 6| Setup of coculture experiments and characterization of bone marrow (BM) cells. (**a**) Setup of coculture experiments: primary cultures of mouse proximal tubule (PT) cells (mPTCs) were obtained from microdissected PT segments of kidneys of *Clcn5*$^{Y/+}$ and *Clcn5*$^{Y/-}$ mice and grown for 7 days. These cells were then cocultivated for 2 days with BM-derived dendritic cells (DCs)/macrophages (BM-DC/MΦ) that were generated by stimulating either wild-type green fluorescent protein (GFP+) or knockout (KO)-BM cells for 7 days with granulocyte-macrophage colony-stimulating factor, resulting in a mixed population of adherent phagocytic cells. (**b**) Staining for GFP (green), 4′,6-diamidino-2-phenylindole (DAPI) (blue), and the mononuclear phagocyte markers CD45 or F4/80 (red) in cocultures of BM-DC/MΦ cells with mPTCs derived from *Clcn5*$^{Y/-}$ mice. (**c**) Progressive upregulation of mRNAs encoding for ClC-5 (*Clcn5*), for the macrophage markers F4/80 (*Adgre1*), CD45 (*Ptprc*), and CD11c (*Itgax*), and for the tunneling nanotube markers myosin Va (*Myo5a*) and M-Sec (*Tnfaip2*) was observed during the differentiation of isolated BM cells into BM-DC/MΦ. $^{**}P < 0.01$ versus d0; $^{***}P < 0.001$ versus d0, Mann-Whitney test. d0, day 0.

hematopoietic system can engraft into various organs, and through the close proximity with diseased cells, they can replace defective enzymes by secretion. In Hurler syndrome (type 1 mucopolysaccharidosis), for example, HSC transplantation has been performed in patients for >30 years.[22] Cystinosis is a lysosomal storage disease caused by the functional loss of the lysosomal transporter cystinosin, resulting in the accumulation of cystine crystals in multiple tissues and cell types. The seminal studies of Cherqui *et al.* have demonstrated the long-term renal protection conferred by BM and HSC transplantation in cystinosis.[10,11] The main effect of transplantation was the reduction of cystine crystals in tissues, whereas improvement of kidney function parameters was only modest, without evidence of rescue of PT endocytic capacity.[10,11] The effects were directly related to the number of phagocytic cells that engrafted in the kidneys.[11]

Here, we tested the effect of BM transplantation in Dent disease, a paradigm of congenital epithelial disorder caused by the loss of a vesicular (endosomal) transporter. Dent disease is particularly suited for an intervention protocol because the defective endocytic uptake by PT cells is readily monitored by the detection of LMW proteins in urine, the most consistent feature of the disease in humans and mice.[5,6,23] Transplantation of healthy BM significantly altered the progression of PT dysfunction in *Clcn5*$^{Y/-}$ mice, as manifested most prominently in the decreased loss of CC16 in urine. This effect was related to the engraftment of BM-derived cells differentiated into mononuclear phagocytes, based on their coexpression of F4/80, CD11c, and CD45. These cells are known to play a role in tissue homeostasis, e.g., by maintaining tolerance of renal antigens or by clearing apoptotic cells.[19] The absence of GFP cells in PT profiles excludes the replacement of damaged tubular cells by BM-derived cells in this model.

The engraftment of BM-derived mononuclear phagocytes resulted in a partial rescue of ClC-5 and megalin expression

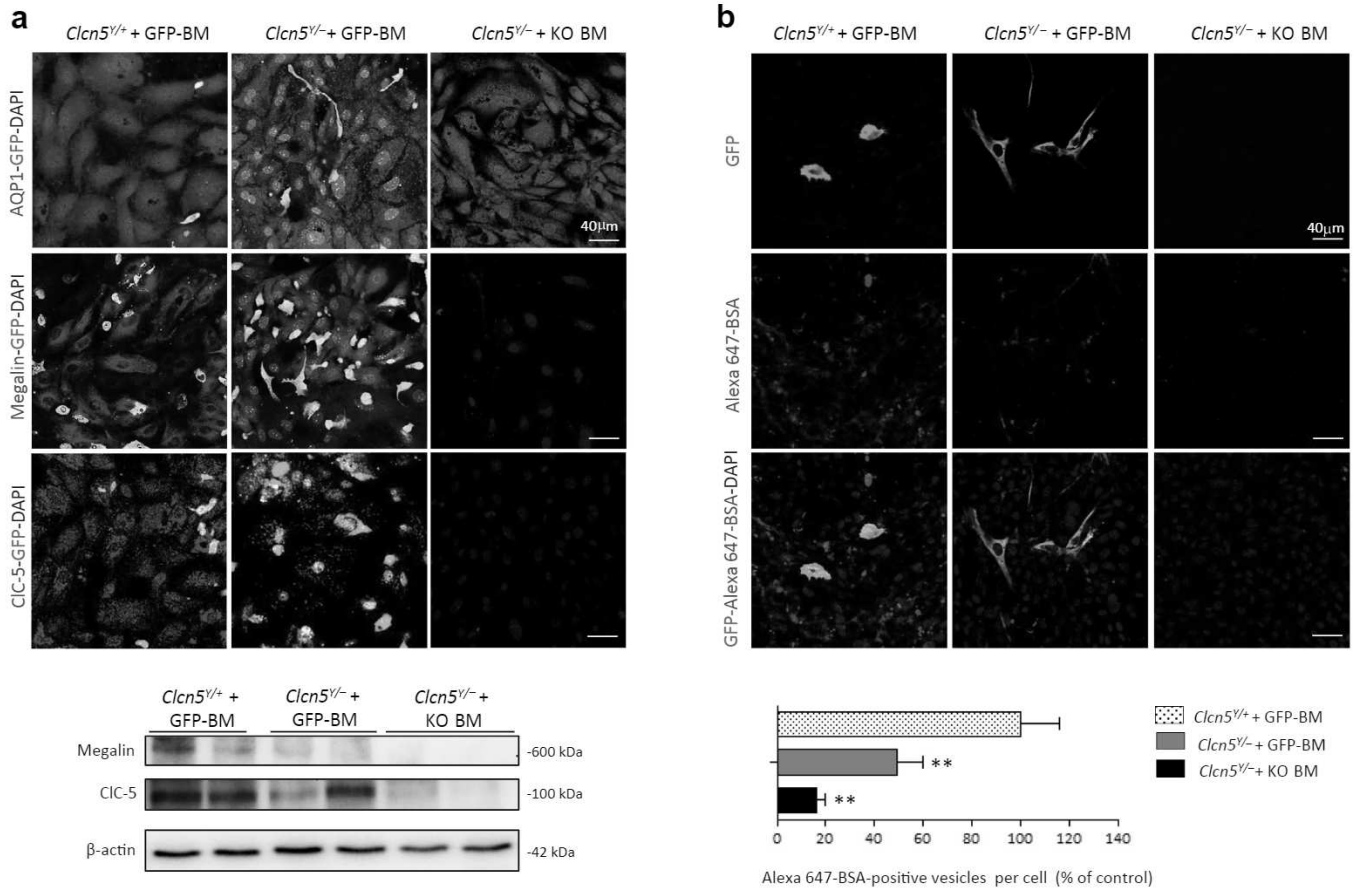

Figure 7 | Cocultures rescue megalin, ClC-5, and endocytosis in *Clcn5*$^{Y/-}$ proximal tubule cells (PTCs). (**a**) Upper panel: Staining for green fluorescent protein (GFP) (green), 4′,6-diamidino-2-phenylindole (DAPI) (blue), AQP-1 (aquaporin-1) (red), megalin (red), and ClC-5 (red) in mouse PTCs (mPTCs) derived from *Clcn5*$^{Y/+}$ and *Clcn5*$^{Y/-}$ kidneys that were cocultured with wild-type (WT) GFP+ or KO-BM–derived BM-DC/MΦ. Coculture with WT GFP+ BM–derived cells rescues the expression of ClC-5 and megalin in the *Clcn5*$^{Y/-}$ mPTCs, whereas no signal is observed in *Clcn5*$^{Y/-}$mPTCs cocultured with KO-BM–derived BM-DC/MΦ. Lower panel: Western blot for megalin and ClC-5 in cell lysates of mPTCs derived from *Clcn5*$^{Y/+}$ and *Clcn5*$^{Y/-}$ mice that were cocultured with WT GFP+ BM–derived cells from *Clcn5*$^{Y/+}$ (WT) or BM-derived cells from *Clcn5*$^{Y/-}$ (KO) mice. (**b**) Upper panel: Uptake of Alexa 647–conjugated bovine serum albumin (BSA) (red channel) in mPTCs derived from *Clcn5*$^{Y/+}$ and *Clcn5*$^{Y/-}$ kidneys that were cocultured with WT GFP+ BM-DC/MΦ or KO-BM-DC/MΦ. A rescue of the endocytic uptake of Alexa 647-BSA is observed in *Clcn5*$^{Y/-}$ mPTCs co-cultured with WT GFP+ BM-derived cells. Lower panel: Quantification of Alexa 647-BSA–positive vesicles per cell. $^{**}P < 0.01$ versus *Clcn5*$^{Y/+}$.

in *Clcn5*$^{Y/-}$ kidneys, with proper expression of the receptor and the endosomal transporter in the apical membrane and subapical domain of PT cells. This observation provides a mechanistic basis for the rescue of endocytosis observed in *Clcn5*$^{Y/-}$ mice. We showed previously that there is no transcriptional defect of megalin in *Clcn5*$^{Y/-}$ kidneys. Instead, the deletion of ClC-5 causes a trafficking defect reflected by the loss of megalin from the brush border.[9] Thus, the transfer of a certain amount of functional ClC-5 and/or megalin (protein or mRNA) to PT cells could be sufficient to rescue megalin expression and receptor-mediated endocytosis (and potentially other apical transport systems such as NaPi-IIa).

Peritoneal macrophages are known to express ClC-5,[24] as do the differentiated BM-derived cells used here, suggesting that the transplanted BM cells express ClC-5 when acquiring their tissue-resident phenotype. This might explain the significant increase of *Clcn5* mRNA and ClC-5 protein expression in PT cells of *Clcn5*$^{Y/-}$ mice transplanted with *Clcn5*$^{Y/+}$ BM compared with controls. The possibility that low-level ClC-5 expression may rescue megalin targeting in PT cells and sustain some level of endocytic uptake is supported by the inverse correlation between rescued *Clcn5* gene expression in the *Clcn5*$^{Y/-}$ kidneys and the level of LMW proteinuria. The fact that the decrease in urinary CC16 does not exactly match the rescue of megalin and ClC-5 protein expression is not really surprising when considering the complexity of receptor-mediated endocytosis, with multiple steps including, but not limited to, those involving megalin and ClC-5.

These observations made *in vivo* are supported by the *in vitro* system based on the coculture of primary PT cells derived from *Clcn5*$^{Y/-}$ kidneys and GFP+ BM cells obtained from *Clcn5* WT and KO mice. The primary cultures of mPTCs have been shown to retain their differentiation and the PT features observed *in vivo*,[25,26] whereas previous exposure of the BM cells to granulocyte-macrophage colony-stimulating factor resulted in their differentiation into functional mononuclear

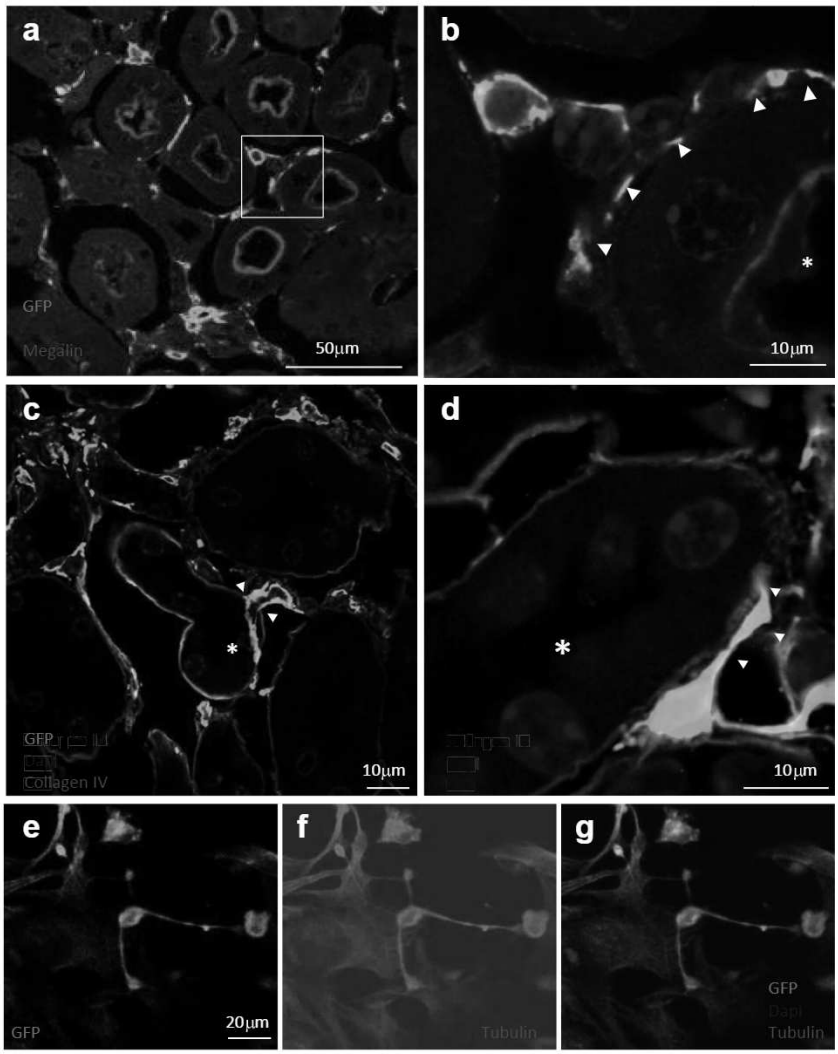

Figure 8| Nanotubes mediate interactions between bone marrow (BM)−derived cells and proximal tubule (PT) cells. (**a**–**d**) Kidney sections of *Clcn5*$^{Y/-}$ mice transplanted with green fluorescent protein (GFP)+ cells showing staining for GFP (green), 4′,6-diamidino-2-phenylindole (DAPI) (blue), and megalin or collagen IV (red). Arrowheads indicate the nanotubular prolongations of the engrafted GFP+ cells contouring the basal membrane of a PT (**b**) and penetrating to collagen IV–positive basement membrane to establish a direct contact with PT cells (**c**,**d**). The asterisk indicates the lumen of the PT. (**e**–**g**) Staining of GFP (green), tubulin (red), and DAPI (blue) and merge (**g**) in mouse PT cells (mPTCs) derived from *Clcn5*$^{Y/-}$ mice cocultivated with GFP+ BM, BM-DC/MΦ cells. Multiple tunneling nanotubes positive for tubulin are identified, establishing connections between BM-derived cells and mPTCs. (Continued)

phagocytes expressing ClC-5 and megalin. The subsequent 2-day coculture confirmed the rescue of megalin and ClC-5 expression, mirrored by the partial recovery of endocytosis.

What could be the mechanism driving the rescue of ClC-5 and megalin expression in the *Clcn5*$^{Y/-}$ PT cells, resulting in the improved phenotype *in vivo* and *in vitro*? The close proximity between transplanted BM-derived cells and PT cells as well as the rescue of ClC-5 and megalin expression in the latter supports the hypothesis of a cell-to-cell transfer of material between the two cell types. We found a greater recruitment of BM-derived cells into the *Clcn5*$^{Y/-}$ kidneys compared with the *Clcn5*$^{Y/+}$ controls, with transplanted cells surrounding PT profiles and establishing close contacts with PT cells. Chronic injury is a prerequisite to stimulate the long-term engraftment of BM-derived cells to the kidneys,[27] suggesting that a homing factor may attract transplanted cells close to diseased PT cells.

In general, intercellular communication can be achieved by paracrine and endocrine signaling, transfer of extracellular vesicles, and cell-to-cell contact mechanisms including tunneling nanotubes.[21,28] The tunneling nanotubes are dynamic, F-actin–based tubular connections that allow communication between relatively distant cells. They operate between various cell types, with a heterogeneous structure reflecting distinct functions. In particular, relatively thick (>0.7-μM diameter) tunneling nanotubes containing microtubules have been described in macrophages and other cell types,[29] with an ability to transfer several types of cargo including vesicles derived from endosomes, plasma membrane components, as well as cytoplasmic molecules.[28] Recent coculture experiments showed that tunneling nanotubes produced by macrophages and extending into fibroblasts mediate a vesicular exchange able to correct the lysosomal

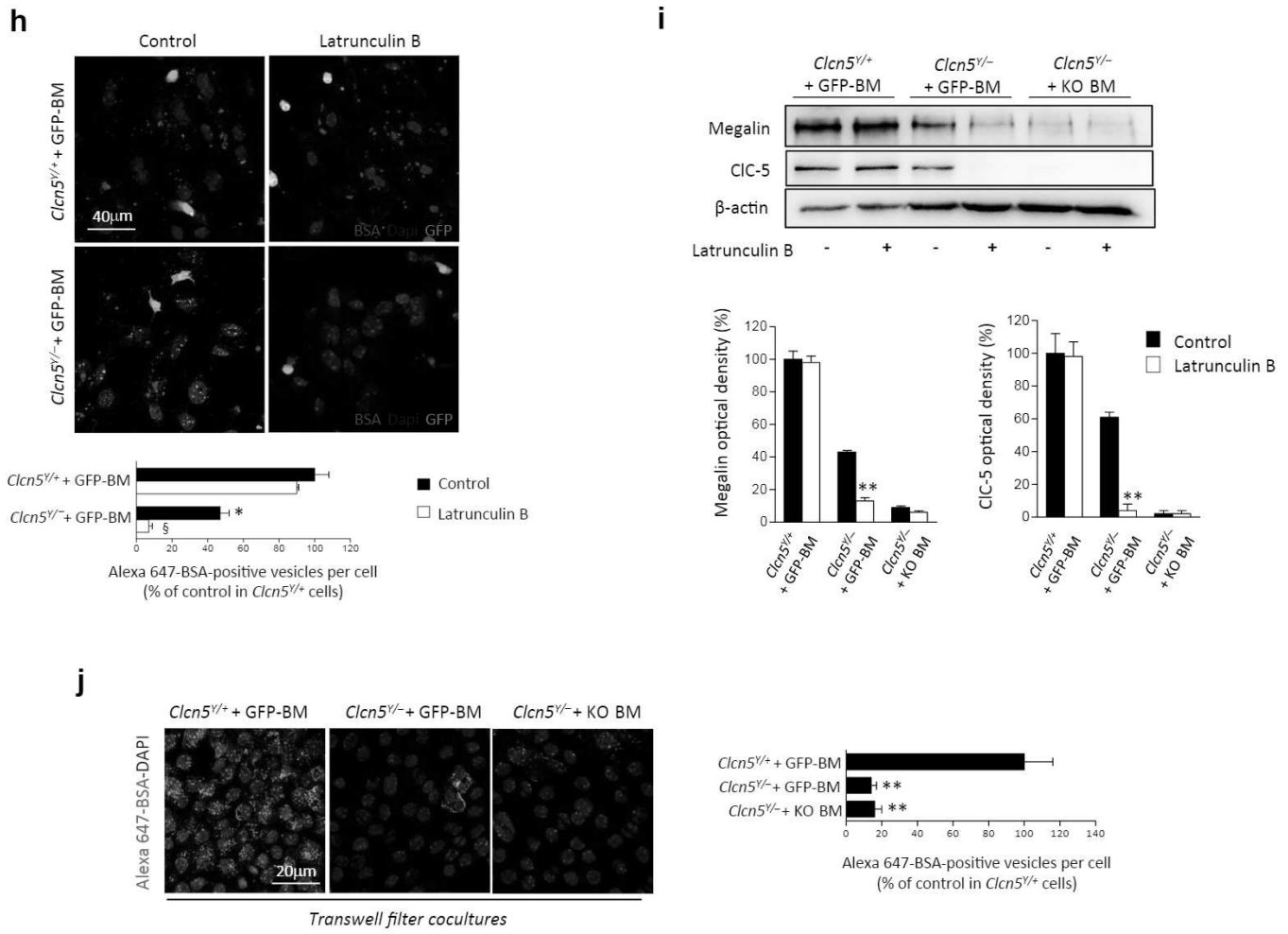

Figure 8| Continued. (**h**) Uptake of Alexa 647-bovine serum albumin (BSA) (red channel) in cocultures of mPTCs derived from *Clcn5*$^{Y/+}$ and *Clcn5*$^{Y/-}$ mice with GFP+ BM–derived cells in the presence of the actin depolymerizing agent Latrunculin B or vehicle (control). Incubation with Latrunculin B inhibits the formation of nanotubes from the GFP+ BM-DC/MΦ, with a lack of rescue of the endocytic uptake of Alexa-BSA in *Clcn5*$^{Y/-}$ mPTCs. *$P < 0.05$ versus control (*Clcn5*$^{Y/+}$ + GFP-BM without Latrunculin B), §$P < 0.05$ versus *Clcn5*$^{Y/-}$ + GFP-BM without Latrunculin B). (**i**) Western blot for megalin and ClC-5 in lysates of mPTCs derived from *Clcn5*$^{Y/+}$ and *Clcn5*$^{Y/-}$ mice, which were cocultured with WT GFP+ or KO-BM–derived cells in the presence or not of Latrunculin B and the quantification of optical densities. Treatment with Latrunculin B almost abolished the rescue of megalin and ClC-5 in the cocultures of *Clcn5*$^{Y/-}$ mPTCs and wild-type (WT)-BM–derived cells. Representative of 2 experiments. **$P < 0.01$ versus control. (**j**) Uptake of Alexa 647-BSA in mPTCs derived from *Clcn5*$^{Y/+}$ and *Clcn5*$^{Y/-}$ kidneys seeded onto the top of collagen-coated transwell filters, with either WT- or KO-BM-DC/MΦ on the basolateral side. Quantification of BSA-positive vesicles per cell reveals no rescue of the endocytic uptake in *Clcn5*$^{Y/+}$ mPTCs cultured with WT BM-derived cells in the basal compartment of the transwell filters. **$P < 0.01$ versus *Clcn5*$^{Y/+}$.

defect in cystinosis.[14] Such macrophage-derived tubular extensions have also been demonstrated *in vivo*, penetrating the tubular basement membrane and delivering cystinosin-containing lysosomes into PT cells.[14]

We observed similar nanotubular extensions between GFP+ BM-derived cells closely surrounding *Clcn5*$^{Y/-}$ PT cells *in vivo* and *in vitro*, with multiple contact points between the transplanted cells and PT cells (Figure 8). It must be noted that the differentiated BM-derived cells expressed M-Sec, a central factor in the induction of plasma membrane protrusion during tunneling nanotube formation,[30] as well as myosin Va, a motor protein that facilitates organelle transport in tunneling nanotubes.[21] Conversely, no rescue of ClC-5 and megalin and no improvement of albumin endocytosis were observed when the cells are separated by a transwell insert system or when the formation of tunneling nanotubes is prevented by treatment with latrunculin B, an actin-depolymerizing drug known to inhibit the development of cell-to-cell connections.[29] Taken together, these results suggest that the establishment of a direct contact between transplanted mononuclear phagocytes and PT cells, via tunneling nanotubes, may enable the transfer of ClC-5 mRNA or protein into *Clcn5*$^{Y/-}$ PT cells, partially rescuing the PT phenotype.

In summary, these data provide the first demonstration that BM transplantation may rescue the epithelial phenotype due to an inherited endosomal defect through direct contact between transplanted BM-derived cells and diseased proximal tubular cells.

MATERIALS AND METHODS

Clcn5 mouse model of Dent disease

Clcn5 mice were generated by deletion of exon VI of *Clcn5* and have been extensively characterized as a well-established model of Dent disease.[9,16] ClC-5 KO males ($Clcn5^{Y/-}$) and WT littermate controls ($Clcn5^{Y/+}$) on a pure C57BL/6 background were used for experiments. BM donors expressed an enhanced GFP under the direction of the human ubiquitin C promotor, leading to ubiquitous GFP expression in all cells (The Jackson Laboratory, Bar Harbor, ME). All BM donor mice were of C57BL/6 background, and only males were used. Mice were bred and housed under specific pathogen-free conditions at the University of Zürich, and all animal experiments were performed according to protocols approved by the local legal authority (Veterinary Office, Canton of Zürich, Switzerland).

Bone marrow transplantation

The *Clcn5* littermates were lethally irradiated (900 cGy) with a cesium source and reconstituted ~6 hours later by tail vein injection of 10×10^6 unfractionated BM cells suspended in Media 199 (Thermo Fisher Scientific) containing 10 mM HEPES, 10 μg/ml DNAse, and 4 μg/ml gentamicin. BM cells were either isolated from the GFP under the direction of the human ubiquitin C promotor or $Clcn5^{Y/-}$ donors ages 8 to 14 weeks. Recipients were randomly distributed among treatment groups and transplanted at the age of 10 weeks. Peripheral blood multilineage chimerism was measured by fluorescence-activated cell sorting at the time of harvest. Cells were stained for CD4, CD8, CD11b, and B220 and acquired at fluorescence-activated cell sorting Canto II or LSRII Fortessa (BD Biosciences, Allschwil, Switzerland).

Urine and plasma collections

Urine samples were collected overnight in metabolic cages with *ad libitum* access to food and drinking water 1 week before BM transplantation and 10 and 16 weeks after transplantation. Urinary calcium, glucose, and creatinine were measured with a Synchron CX3 Delta System (Beckman Coulter, Nyon, Switzerland), and urinary CC16 was measured by an enzyme-linked immunosorbent assay kit (Biomatik, Wilmington, DE).

Kidney sampling

Mice were anesthetized using an isoflurane vaporizer and perfused through the right ventricle with a 0.9% NaCl solution containing heparin (5000 U/ml), 1% procaine HCl (lidocaine), and 16% $CaCl_2$. Then the left kidney was clamped and the right kidney was fixed by infusion of 3% paraformaldehyde dissolved in 0.1 M Na-cacodylate. One half of the unfixed kidney was used for protein isolation and the other half for RT-qPCR analysis. The fixed kidney was kept for 1 hour in 3% paraformaldehyde on ice and then in 1% paraformaldehyde overnight. After washing in phosphate-buffered saline (PBS) and soaking in 30% sucrose, the kidneys were embedded in Tissue-Tek OCT medium (VWR, Radnor, PA).

Isolation and primary cultures of mouse PT cells

Primary cultures of mouse PT cells (mPTCs) were prepared from sex-matched $Clcn5^{Y/-}$ mice transplanted with KO-BM cells or GFP-BM cells and from $Clcn5^{Y/+}$ mice transplanted with GFP+ BM cells, as described previously.[20,25,26] Confluent monolayers of mPTCs expanded from the tubular fragments after 6 to 7 days. All experiments were performed on nonpassaged, confluent monolayers grown on collagen-coated filters.

Cultures of BM cells and coculture experiments

BM cells were isolated from femurs of GFP-expressing $Clcn5^{Y/+}$ mice and of $Clcn5^{Y/-}$ mice and were differentiated in the presence of the granulocyte-macrophage colony-stimulating factor (30 ng/ml) for 7 days, as previously described.[31]

For contact coculture assays, 1×10^5 mPTCs were plated with 1×10^5 GFP+ or KO-BM-derived cells in 10-cm culture dishes. Cells were incubated for 2 days at 37°C, harvested using trypsin, pelleted, and resuspended in PBS with 2% fetal bovine serum.

For the latrunculin B assay, 1×10^5 mPTCs were seeded with 1×10^5 GFP+ or KO-BM–derived cells in 24-well plates (Corning Life Sciences, Big Flats, NY) in presence of 5 μM of latrunculin B for 2 days at 37°C, as previously described.[32] The albumin endocytic assay was performed (see the following), and the cells were further processed for immunofluorescence staining.

For the transwell coculture assay, mPTCs were seeded on the top of collagen-coated polytetrafluoroethylene filter membranes (0.33 cm^2, 0.4-μm pore size; Transwell-COL, Costar, Corning Life Sciences) and GFP+ BM-derived cells were plated on the basolateral side of collagen-coated 24-well plates for 2 days at 37°C. The albumin endocytic assay was then performed on the mPTCs, and the cells were processed for immunofluorescence staining.

Albumin endocytic uptake

The endocytosis assay was performed on monolayers of mPTCs, as described previously.[26] Briefly, monolayers of mPTCs were incubated with either 0.5 mg/ml Alexa 488-BSA or Alexa 647-BSA (both from Thermo Fisher Scientific) for 15 minutes at 37°C. After the incubation, primary cultures were washed and fixed in 4% paraformaldehyde and counterstained with 3 μM 4′,6-diamidino-2-phenylindole (DAPI) (D1306, Thermo Fischer Scientific). The slides were mounted in Prolong Gold Anti-fade reagent (P36930, Thermo Fisher Scientific), acquired on a Leica SP5 confocal laser scanning microscope (Leica, Heerbrugg, Switzerland). Quantitative image analysis was performed by randomly selecting 2 to 4 fields containing ~50 cells, using the same setting parameters (i.e., laser power, offset gain, and detector amplification below pixel saturation). The number of albumin-positive vesicles was determined using AnalySIS software (Soft Imaging Systems GmbH, Muenster, Germany).

qPCR

Total RNA was extracted from kidneys using the Aurum Total RNA Fatty and Fibrous Tissue Kit (Bio-Rad, Hercules, CA) according to manufacturer's protocol. DNAse I treatment was performed to eliminate genomic DNA contamination. One microgram of RNA was used to perform the reverse transcriptase reaction with an iScript cDNA Synthesis Kit (Bio-Rad). Changes in target gene mRNA levels were determined by relative reverse transcriptase qPCR with a CFX96 Real-Time PCR Detection System (Bio-Rad), using iQ SYBR Green Supermix (Bio-Rad). Reverse transcriptase qPCR analyses were performed in duplicate. Specific primers were designed using Primer3 (http://simgene.com/Primer3) (Supplementary Table S1). PCR conditions were 95°C for 3 minutes followed by 40 cycles of 15 s at 95°C and 30 s at 60°C. The PCR products were sequenced with the BigDye terminator kit (PerkinElmer Applied Biosystems, Waltham, MA; Thermo Fisher Scientific). The efficiency of each set of primers was determined by dilution curves (Supplementary Table S1). The relative changes in target over *Gapdh* mRNAs was calculated using the $2^{\Delta ct}$ formula.

Antibodies

The following antibodies were used: rabbit anti-GFP (Thermo Fisher Scientific), goat anti-GFP (Sicgen Research and Development in Biotechnology, Carcavelos, Portugal), rabbit anti–aquaporin-1 (Millipore, Temecula, CA), rabbit anti-Napi-IIa (a gift from C.A. Wagner, University of Zürich), sheep anti-megalin (a gift from Dr. P. Verroust and Dr. R. Kozyraki, INSERM, Paris), rabbit anti-ClC-5 (a gift from J. Loffing, University of Zürich), rat anti-F4/80 (ABD Serotec Bio-Rad, Puchheim, Germany), hamster anti-CD11c (Bio-Rad), rat anti-CD45 (Bio-Rad), rabbit anti–α-smooth muscle actin (Abcam, Cambridge, UK), mouse anti–β-actin (Sigma-Aldrich), rabbit anti-Rab5 (Abcam), mouse anti–α-tubulin (Sigma-Aldrich), and rabbit anti-collagen IV antibody (Abcam). Secondary antibodies were labeled with Alexa 488, Alexa 633, or Dylight649.

Immunofluorescence and confocal microscopy

Six-micrometer mouse kidney sections were quenched with 50 mM NH_4Cl, blocked with 0.5% BSA in PBS Ca/Mg (D1283, Sigma-Aldrich) for 30 minutes and stained with primary antibodies diluted in blocking buffer overnight at 4°C. After 2 washes in 0.1% Tween 20 (vol/vol in PBS), the slides were incubated with corresponding fluorophore-conjugated secondary antibodies (Invitrogen, Carlsbad, CA and Thermo Fisher Scientific) diluted in blocking buffer at room temperature for 1 hour and counterstained with 3 μM 4′ ,6-diamidino-2-phenylindole (DAPI) (D1306, Thermo Fischer Scientific). The slides were mounted in Prolong Gold Antifade reagent (P36930, Thermo Fisher Scientific), acquired on a Leica SP5 confocal laser scanning microscope. Quantitative image analysis was performed by randomly selecting ~3 visual fields per each slide that included at least 2 to 4 PT sections, using the same setting parameters. The number of GFP+ cells/mm^2 was quantified by means of Volocity software (I40250, PerkinElmer), and the distance of GFP+ cells from PT cells (megalin-positive brush border membrane) was measured using Huygens software (Scientific Volume Imaging, Hilversum, the Netherlands).

The cells were fixed for 10 minutes in 4% paraformaldehyde (Sigma-Aldrich,) in PBS, and permeabilized and quenched for 30 minutes in blocking buffer (50 mM NH_4Cl, 0.1% (wt/vol) saponin, 3% (wt/vol) BSA in PBS). The cells were then incubated for 2 hours with the primary antibody, washed 6 times in PBS, incubated for 1 hour with the Alexa-labeled secondary antibody, and mounted on Vectashield covered coverslips (Vector Laboratories, Burlingame, CA) to be acquired on a Leica SP5 confocal laser scanning microscope.

Immunoblotting

Proteins were extracted from frozen kidneys lysed in RIPA buffer (Sigma) containing protease inhibitors (Roche Diagnostics, Mannheim, Germany), followed by a brief sonication and centrifugation at 16,000*g* for 1 minute at 4°C. Protein concentration was determined using the Pierce BCA protein assay (Thermo Fisher Scientific). Immunoblotting and quantification of the signals were performed as described previously.[25,26]

Statistics

The effect of BM transplantation was analyzed by comparing parameters by Kruskal-Wallis, Mann-Whitney, or Wilcoxon signed rank tests, as indicated. Differences between unpaired groups were assessed using the Mann-Whitney test, and correlation between *Clcn5* mRNA expression and urinary loss of CC16 was assessed with GraphPad Prism (GraphPad Software, La Jolla, CA). $P < 0.05$ was considered significant.

DISCLOSURE

All the authors declared no competing interests.

ACKNOWLEDGMENTS

This work was supported by the European Community's Seventh Framework Programme (FP7/2007-2013) under grant agreement no. 305608 (EURenOmics), the Cystinosis Research Foundation (Irvine, CA), the Zürich Center for Integrative Human Physiology (ZIHP), the Swiss National Science Foundation project grant 31003A_169850; the KFSP RADIZ (Rare Disease Initiative Zürich), and MINZ (Molecular Imaging Zürich) from the University of Zürich, Zürich, Switzerland.

SUPPLEMENTARY MATERIAL

Table S1. Primer sequences used in real-time qPCR analyses. The efficiency of each set of primers was determined by dilution curves.

Figure S1. Expression of ClC-5 in bone marrow–derived cells and in subapical vesicles of proximal tubule cells. (**A**) Confocal microscopy images showing staining for F4/80 (green), ClC-5 (red), and 4′,6-diamidino-2-phenylindole (DAPI) (blue) in the kidneys of *Clcn5* mice transplanted with wild-type green fluorescent protein-labeled bone marrow (GFP-BM) cells. The ClC-5 signal was detected in BM-derived cells (arrowheads) in the kidneys of transplanted $Clcn5^{Y/+}$ (**top panels**) and $Clcn5^{Y/-}$ (**bottom panels**) mice. Note the rescue of ClC-5 expression in both the brush border and subapical vesicles of proximal tubule cells in the transplanted kidneys of $Clcn5^{Y/-}$ mice (asterisk, lumen of proximal tubule cells). (**B**) Representative Western blots for megalin, ClC-5, and β-actin in BM-derived dendritic cells/macrophages (BM-DC/MΦ) at days 0 and 6 of culture in medium containing granulocyte-macrophage colony-stimulating factor (30 ng/ml). On differentiation, BM-DC/MΦ express megalin and ClC-5. Kidney extracts are shown as positive controls.

Figure S2. Colocalization of megalin and ClC-5 in bone marrow–derived cells. Confocal microscopy images showing staining for megalin (red), ClC-5 (green), and 4′,6-diamidino-2-phenylindole (DAPI) (blue) in the kidneys of $Clcn5^{Y/+}$ (**top panels**) and $Clcn5^{Y/-}$ (**bottom panels**) mice transplanted with green fluorescent protein-labeled bone marrow (GFP-BM) cells. Partially overlapping megalin and ClC-5 signals are detected in proximal tubule cells as well as in BM-derived cells and in the nanotubular structures (arrowheads, particularly in the transplanted kidneys from $Clcn5^{Y/-}$ mice).

Figure S3. Engraftment efficiency of bone marrow–derived cells in transplanted $Clcn5^{Y/+}$ and $Clcn5^{Y/-}$ kidneys. Confocal microscopy images showing staining for markers of dendritic cells and macrophages F4/80 (**upper panels**), CD45 (**middle panels**), CD11c (**lower panels**), and 4′,6-diamidino-2-phenylindole (DAPI) (blue) in the kidneys of $Clcn5^{Y/+}$ and $Clcn5^{Y/-}$ mice transplanted with wild-type (WT) green fluorescent protein-labeled bone marrow (GFP)+ or $Clcn5^{Y/-}$ knockout bone marrow (KO-BM)–derived cells. A greater engraftment of BM-derived cells is consistently observed in the kidneys of $Clcn5^{Y/-}$ mice compared with $Clcn5^{Y/+}$ mice, whereas the engraftment efficiency is similar in WT GFP+ and KO-BM-derived cells in the kidneys of $Clcn5^{Y/-}$ mice. Quantification was performed on >200 cells per condition, distributed in 5 to 10 fields. The Mann-Whitney test was used to assess the difference between groups. $^{**}P < 0.01$ versus $Clcn5^{Y/+}$ + GFP-BM, $^{***}P < 0.001$ versus $Clcn5^{Y/+}$ + GFP-BM.

Figure S4. Detection of green fluorescent protein (GFP)+ structures in proximal tubule cells from transplanted $Clcn5^{Y/-}$ kidneys and in coculture. Confocal microscopy images showing staining for GFP (green) and 4′,6-diamidino-2-phenylindole (DAPI) (blue) in proximal tubule cells in the kidneys of $Clcn5^{Y/-}$ mice transplanted with GFP+ bone marrow (BM)–derived cells (**left panels**) and in primary cultured mouse proximal tubule cells (mPTCs) from $Clcn5^{Y/-}$ kidneys that were cocultured with BM-derived dendritic cells/macrophages

(**right panels**). **Lower panels** are high-magnification insets shown in the **upper panels**. The mPTCs are delineated by dashed lines. Asterisk, PT lumen; Mag, magnification.

Supplementary material is linked to the online version of the paper at www.kidney-international.org.

REFERENCES

1. De Matteis MA, Luini A. Mendelian disorders of membrane trafficking. *N Engl J Med*. 2011;365:927–938.
2. Eckardt KU, Coresh J, Devuyst O, et al. Evolving importance of kidney disease: from subspecialty to global health burden. *Lancet*. 2013;382:158–169.
3. Nielsen R, Christensen EI, Birn H. Megalin and cubulin in PT protein reabsorption: from experimental models to human disease. *Kidney Int*. 2016;89:58–67.
4. Devuyst O, Igarashi T. Renal Fanconi syndrome, Dent's disease and Bartter's syndrome. In: Thakker RV, Whyte MP, Eisman JA, Igarashi T, eds. *Genetics of Bone Biology and Skeletal Disease*. 2nd ed. Amsterdam: Elsevier Inc.; 2015:553–567.
5. Devuyst O, Thakker RV. Dent's disease. *Orphanet J Rare Dis*. 2010;5:28.
6. Devuyst O, Christie PT, Courtoy PJ, et al. Intra-renal and subcellular distribution of the human chloride channel, CLC-5, reveals a pathophysiological basis for Dent's disease. *Hum Mol Genet*. 1999;8:247–257.
7. Stauber T, Jentsch TJ. Chloride in vesicular trafficking and function. *Annu Rev Physiol*. 2013;75:453–477.
8. Piwon N, Gunther W, Schwake M, et al. ClC-5 Cl- -channel disruption impairs endocytosis in a mouse model for Dent's disease. *Nature*. 2000;408:369–373.
9. Christensen EI, Devuyst O, Dom G, et al. Loss of chloride channel ClC-5 impairs endocytosis by defective trafficking of megalin and cubilin in kidney proximal tubules. *Proc Natl Acad Sci U S A*. 2003;100:8472–8477.
10. Syres K, Harrison F, Tadlock M, et al. Successful treatment of the murine model of cystinosis using bone marrow cell transplantation. *Blood*. 2009;114:2542–2552.
11. Yeagy BA, Harrison F, Gubler MC, et al. Kidney preservation by bone marrow cell transplantation in hereditary nephropathy. *Kidney Int*. 2011;79:1198–1206.
12. Gahl WA, Thoene JG, Schneider JA. Cystinosis. *N Engl J Med*. 2002;347:111–121.
13. Harrison F, Yeagy BA, Rocca CJ, et al. Hematopoietic stem cell gene therapy for the multisystemic lysosomal storage disorder cystinosis. *Mol Ther*. 2013;21:433–444.
14. Naphade S, Sharma J, Gaide Chevronnay HP, et al. Lysosomal cross-correction by hematopoietic stem cell-derived macrophages via tunneling nanotubes. *Stem Cells*. 2015;33:301–309.
15. Pinkernell K. Cellular therapies: what is still missing? *Kidney Int*. 2011;79:1161–1163.
16. Wang SS, Devuyst O, Courtoy PJ, et al. Mice lacking renal chloride channel, CLC-5, are a model for Dent's disease, a nephrolithiasis disorder associated with defective receptor-mediated endocytosis. *Hum Mol Genet*. 2000;9:2937–2945.
17. François S, Bensidhoum M, Mouiseddine M, et al. Local irradiation not only induces homing of human mesenchymal stem cells at exposed sites but promotes their widespread engraftment to multiple organs: a study of their quantitative distribution after irradiation damage. *Stem Cells*. 2006;24:1020–1029.
18. Morigi M, Imberti B, Zoja C, et al. Mesenchymal stem cells are renotropic, helping to repair the kidney and improve function in acute renal failure. *J Am Soc Nephrol*. 2004;15:1794–1804.
19. Weisheit CK, Engel DR, Kurts C. Dendritic cells and macrophages: sentinels in the kidney. *Clin J Am Soc Nephrol*. 2015;10:1841–1851.
20. Terryn S, Jouret F, Vandenabeele F, et al. A primary culture of mouse proximal tubular cells established on collagen-coated membranes. *Am J Physiol Renal Physiol*. 2007;293:F476–F485.
21. Rustom A, Saffrich R, Markovic I, et al. Nanotubular highways for intercellular organelle transport. *Science*. 2004;303:1007–1010.
22. Aldenhoven M, Wynn RF, Orchard PJ, et al. Long-term outcome of Hurler syndrome patients after hematopoietic cell transplantation: an international multicenter study. *Blood*. 2015;125:2164–2172.
23. Bernard AM, Thielemans NO, Lauwerys RR. Urinary protein 1 or Clara cell protein: a new sensitive marker of proximal tubular dysfunction. *Kidney Int*. 1994;47:S34–S37.
24. Alex P, Ye M, Zachos NC, et al. Clcn5 knockout mice exhibit novel immunomodulatory effects and are more susceptible to dextran sulfate sodium-induced colitis. *J Immunol*. 2010;184:3988–3996.
25. Raggi C, Luciani A, Nevo N, et al. Dedifferentiation and aberrations of the endolysosomal compartment characterize the early stage of nephropathic cystinosis. *Hum Mol Genet*. 2014;23:2266–2278.
26. Luciani A, Sirac C, Terryn S, et al. Impaired lysosomal function underlies monoclonal light chain associated renal Fanconi syndrome. *J Am Soc Nephrol*. 2016;27:2049–2061.
27. Yeagy BA, Cherqui S. Kidney repair and stem cells: a complex and controversial process. *Pediatr Nephrol*. 2011;26:1427–1434.
28. Abounit S, Zurzolo C. Wiring through tunneling nanotubes-from electrical signals to organelle transfer. *J Cell Sci*. 2012;125:1089–1098.
29. Abounit S, Delage E, Zurzolo C. Identification and characterization of tunneling nanotubes for intercellular trafficking. *Curr Protoc Cell Biol*. 2015;67:12.10.1–12.10.21.
30. Kimura S, Hase K, Ohno H. The molecular basis of induction and formation of tunnelling nanotubes. *Cell Tissue Res*. 2013;352:67–76.
31. Madaan A, Verma R, Singh AT, et al. A stepwise procedure for isolation of murine bone marrow and generation of dendritic cells. *J Biol Methods*. 2014;1:e1.
32. Takahashi A, Kukita A, Li YJ, et al. Tunneling nanotube formation is essential for the regulation of osteoclastogenesis. *J Cell Biochem*. 2013;114:1238–1247.